

Isomerism of Assembled Iron Complex Bridged by 1,2-Di(4-pyridyl)ethane and Its Solid-to-Solid Transformation Accompanied by a Change of Electronic State

Takaki Morita,[1] Yoritaka Asada,[1] Tsutomu Okuda,[2] and Satoru Nakashima*[3]

[1]Department of Chemistry, Graduate School of Science, Hiroshima University, 1-3-1 Kagamiyama, Higashi-Hiroshima 739-8526

[2]Department of Bio-Recycling, Faculty of Engineering, Hiroshima Kokusai Gakuin University, 6-20-1 Nakano, Aki-ku, Hiroshima 739-0321

[3]Natural Science Center for Basic Research and Development (N-BARD), Hiroshima University, 1-4-2 Kagamiyama, Higashi-Hiroshima 739-8526

Received December 7, 2005; E-mail: snaka@hiroshima-u.ac.jp

Three supramolecular isomers of an Fe–NCS complex and two isomers of an Fe–NCSe complex bridged by 1,2-di(4-pyridyl)ethane have been obtained. ^{57}Fe Mössbauer spectroscopy revealed a drastic change in the QS value by changing the structure and by changing NCS to NCSe. Solid-to-solid transformation was observed, accompanied by a drastic change in the QS value.

Self-assembled coordination polymers containing transition-metal ions and organic bridging ligands have attracted intensive interests because of their potential abilities for selective inclusion and transformation of ions and molecules.[1–20] Supramolecular isomerism, the existence of more than one superstructure for a given set of components, is of particular importance because the superstructure plays an essential role in determining the properties of crystalline materials.[21]

The spin-crossover phenomenon of the assembled complexes is interesting.[22–26] The phenomenon depends on the crystal structure. The interpenetration structure of $[Fe(NCS)_2(tvp)_2]\cdot CH_3OH$ (tvp = *trans*-1,2-di(4-pyridyl)ethylene) shows spin-crossover behavior,[24] while the 2D structure of $[Fe(NCS)_2(tvp)_2]\cdot 0.5(tvp\cdot 2EtOH)$ does not show it.[27] As a basis of our investigations to synthesize spin-crossover assembled complexes, it is important to synthesize several structures of the same components.

From these points, it is important to synthesize assembled coordination polymers using 1,2-di(4-pyridyl)ethane (bpa) as a bridging ligand, because the ligand has an *anti–gauche* isomer; therefore, there is a possibility to have a variety of supramolecular isomers depending on the isomer of bpa. Actually, there are many structures in the bpa complexes,[12,17,18,28] but only the 1D structure is reported in the Fe–bpa–NCS complex.[17] If supramolecular isomers are obtained, it becomes interesting to study the change of electronic state of the metal ion depending on the isomer of bpa and its assembled structure.

In the present study, we report three supramolecular isomers of an Fe–NCS complex and two isomers of an Fe–NCSe complex bridged by bpa. We found a drastic change in the QS value of the ^{57}Fe Mössbauer spectra by changing the structure and by changing NCS to NCSe. We also report a solid-to-solid transformation phenomenon, accompanied by a drastic change in the QS value.

Experimental

$FeSO_4\cdot 7H_2O$ (278 mg) and NaNCS (162 mg) (or KNCSe (288 mg)) were dissolved in water (20 mL). To the solution, a mixed solvent (40 mL) of ethanol (or methanol, 1-propanol) and water was added, and then an ethanol (or methanol, 1-propanol) solution (20 mL) of bpa (368 mg) was added carefully. From this solution, three types of pale yellow crystals appeared of the same color. The shape of the crystals for the 1D structure has bad symmetry, while that for the interpenetration structure is a pillar-like crystal. Anal. Calcd for $C_{26}H_{24}N_6S_2Fe$: C, 57.8; H, 4.5; N, 15.6; S, 11.9%. Found for the 1D structure of $Fe(NCS)_2(bpa)_2$: C, 58.2; H, 3.3; N, 16.0; S, 11.4%. Calcd for $C_{26}H_{24}N_6Se_2Fe$: C, 49.2; H, 3.8; N, 13.3%. Found for the 1D structure of $Fe(NCSe)_2(bpa)_2$: C, 49.2; H, 3.6; N, 13.4%. Elemental analyses did not show the exact values for the 2D grid and interpenetration structures both in NCS and NCSe complexes. The reason will be discussed later.

Single crystals for X-ray crystallography were obtained by the above method. All measurements were made on a Mac Science DIP2030 imaging plate area detector using graphite monochromated Mo Kα radiation at 130 or 200 K. The cell parameters and intensities for the reflection were estimated by the program package of MacDENZO.[29] The crystal structures were solved by direct methods and expanded using Fourier techniques. The non-hydrogen atoms were refined anisotropically, while hydrogen atoms were refined isotropically. All calculations were performed with the CrystalStructure crystallographic software packages of Rigaku and Molecular Structure Corporation.[30,31] Table 1 summarizes the crystallographic data and experimental details. Crystallographic data have been deposited with Cambridge Crystallographic Data Centre: Deposition numbers CCDC 295987–295990. Copies of the data can be obtained free of charge via http://

Published on the web May 12, 2006; DOI: 10.1246/bcsj.79.738

Table 1. Structural Data and Refinement

Sample	$[Fe(NCS)_2(bpa)_2]\cdot EtOH$ 2D grid	$[Fe(NCS)_2(bpa)_2]\cdot EtOH$ Interpenetration	$[Fe(NCSe)_2(bpa)_2]$ 1D	$[Fe(NCSe)_2(bpa)_2]\cdot EtOH$ Interpenetration
Formula	$C_{28}H_{30}N_6OS_2Fe$	$C_{28}H_{30}N_6OS_2Fe$	$C_{26}H_{24}N_6Se_2Fe$	$C_{28}H_{30}N_6OSe_2Fe$
Formula weight	586.55	586.55	634.28	680.35
Space group	*P*1	*Ibam*	*Cc*	$P2_1/a$
a/Å	8.2740(2)	13.2420(7)	19.8440(8)	13.2660(5)
b/Å	8.8390(2)	16.8644(9)	10.0760(3)	16.8460(7)
c/Å	10.0860(2)	16.8296(8)	15.3390(8)	16.7030(8)
α/°	93.235(2)	90	90	90
β/°	100.546(2)	90	112.783(2)	90.027(2)
γ/°	101.550(1)	90	90	90
V/Å^3	707.16(3)	3758.4(3)	2827.7(2)	3732.8(3)
Z	1	4	4	4
T/K	130	200	130	130
λ/Å	0.71069	0.71069	0.71069	0.71069
ρ_{calcd}/g cm^{-3}	1.377	1.037	1.490	1.211
μ(Mo Kα)/cm^{-1}	7.13	5.36	31.32	23.79
Data ($I > 3.00\sigma(I)$)	2958	1432	2414	4962
R[a)]	0.049	0.127	0.043	0.140
R_w[b)]	0.059	0.176	0.043	0.161

a) $R = \Sigma||F_O| - |F_C||/\Sigma|F_O|$. b) $R_w = [\Sigma w(|F_O| - |F_C|)^2/\Sigma wF_O^2]^{1/2}$.

www.ccdc.cam.ac.uk/conts/retrieving.html (or from the Cambridge Crystallographic Data Centre, 12, Union Road, Cambridge, CB2 1EZ, UK; Fax: +44 1223 336033; e-mail: deposit@ccdc.cam.ac.uk).

Powder X-ray diffraction patterns were measured by using graphite-monochromated Cu Kα radiation (Rigaku) at room temperature and with increasing temperature.

A ^{57}Co(Rh) source moving in a constant-acceleration mode was used for ^{57}Fe Mössbauer spectroscopic measurements. ^{57}Fe Mössbauer spectra at 78 K and room temperature were obtained by using a Wissel spectrometer. The ^{57}Fe Mössbauer parameters were obtained by least-squares fitting to Lorentzian peaks. The isomer shift values are referred to metallic iron.

Results and Discussion

Single crystals were obtained by the diffusion method shown in the Experimental section. The use of bpa as a bridging ligand plays a key role to the formation of supramolecular isomers because this ligand has an *anti–gauche* isomer that reflects the assembled structure. Depending on the solvent for bpa, several types of crystals were obtained. $FeSO_4\cdot 7H_2O$ and NaNCS (or KNCSe) were always dissolved in water. The use of water or MeOH as the solvent for bpa led to the 1D structure, while PrOH led to the interpenetration structure. Interestingly, the use of EtOH as the solvent for bpa led to the 2D grid structure as well as the above two structures. On the other hand, the 2D grid structure was not obtained in the case of NCSe. The diffusion speed of the two solvents is controlled by the proportion of hydrophobic groups in alcohol. Therefore, it is explained that the assembled structure is controlled by the diffusion speed and the size of the guest solvent molecule, i.e., the 1D structure is obtained in relatively fast diffusion conditions and the structure does not include solvent, while the interpenetration structure is obtained in slow diffusion conditions and a suitable size of the guest molecule is included in the pore.

All the measurements were performed in the hydrocarbon, because compounds except for the 1D structure were readily destroyed by exposure to air. This is due to the removal of the solvent molecule from the crystal. For this reason, the elemental analyses did not show the exact values except for the 1D structure. By removing the solvent molecule the structure changes to another one. This structural change will be discussed later.

The 1D structure of $[Fe(NCS)_2(bpa)_2]$ has already been reported.[17] We also obtained the same 1D structure for the NCS complex, which was confirmed by the X-ray structural analysis. This 1D structure consists of a *gauche* isomer of bpa, which is the same as the reported one. The solvent molecule is not included in this structure. The bond distances and angles are the same as the reported values.

Figures 1 and 2 show the ORTEP drawings of the 2D grid structure and interpenetration structure including EtOH, re-

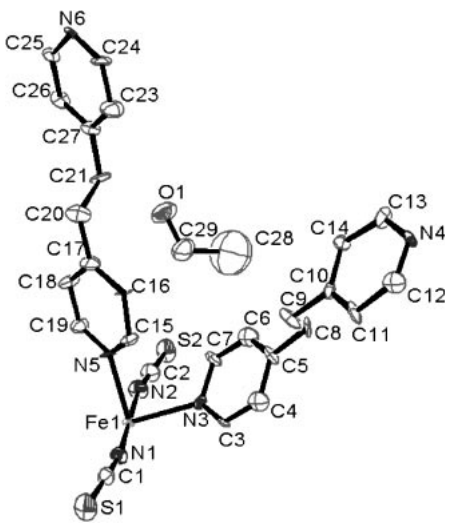

Fig. 1. ORTEP drawing of the 2D grid structure of $[Fe(NCS)_2(bpa)_2]\cdot EtOH$ at 130 K.

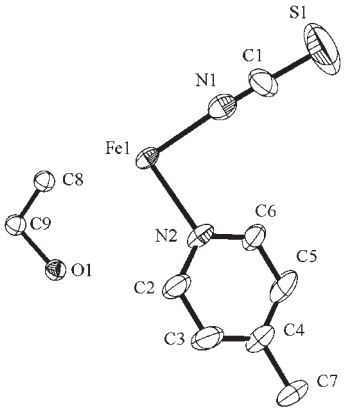

Fig. 2. ORTEP drawing of the interpenetration structure of $[Fe(NCS)_2(bpa)_2]\cdot EtOH$ at 200 K.

Table 2. Selected Bond Distances (Å) and Angles (°) for the 2D Grid Structure of $[Fe(NCS)_2(bpa)_2]\cdot EtOH$

Fe1–N1	2.08(1)	Fe1–N2	2.14(1)
Fe1–N3	2.28(1)	Fe1–N4[a)]	2.25(1)
Fe1–N5	2.27(1)	Fe1–N6[b)]	2.24(1)
N1–Fe1–N3	90.7(5)	N1–Fe1–N4[a)]	90.3(5)
N1–Fe1–N5	90.7(4)	N1–Fe1–N6[b)]	90.4(4)
N2–Fe1–N3	89.5(4)	N2–Fe1–N4[a)]	89.4(4)
N2–Fe1–N5	89.3(4)	N2–Fe1–N6[b)]	89.6(4)
N3–Fe1–N5	95.5(5)	N3–Fe1–N6[b)]	84.6(4)
N4[a)]–Fe1–N5	84.7(4)	N4[a)]–Fe1–N6[b)]	95.2(4)
N1–Fe1–N2	179.8(5)	N3–Fe1–N4[a)]	178.9(4)
N5–Fe1–N6[b)]	179.0(4)	Fe1–N1–C1	168(1)
Fe1–N2–C2	169(1)	N1–C1–S1	178(1)
N2–C2–S2	179(1)		

a) Symmetry operator: $x+1, y-1, z$. b) Symmetry operator: $x, y+1, z-1$.

Table 3. Selected Bond Distances (Å) and Angles (°) for the Interpenetration Structure of $[Fe(NCS)_2(bpa)_2]\cdot EtOH$

Fe1–N1	2.15(1)	Fe1–N2	2.242(7)
N1–Fe1–N2	89.0(3)	Fe1–N1–C1	175.0(13)
N1–C1–S1	179.2(17)		

spectively. The crystallographic data are shown in Table 1. The selected bond distances and angles are shown in Tables 2 and 3, respectively. X-ray structural analysis revealed that the crystal obtained from the water–PrOH mixed solvent has an interpenetration structure, but we could not determine the solvent molecule. The 2D grid structure and interpenetration structure consist of an *anti* isomer of bpa, which is in significant contrast to the corresponding 1D structure. These 2D grid and interpenetration structures include the solvent molecule. The iron atoms are coordinated by four pyridine nitrogen donors in the basal plane and two thiocyanate nitrogen donors in the axial sites. The *cis* N–Fe–N bond angles deviate slightly from 90°, indicative of a slightly distorted environment in the 2D grid structure, while the angles do not significantly deviate in the interpenetration structure. The NCS ligands coordinate to the Fe atom in a slightly bent fashion in the 2D grid structure, while the NCS ligands coordinate to the Fe atom in a parallel fashion in the interpenetration structure. These bendings are smaller compared with the case of the 1D structure. The NCS ligands themselves are almost linear. The Fe–N(NCS) and Fe–N(bpa) distances are typical values in the Fe^{II} high-spin complexes.

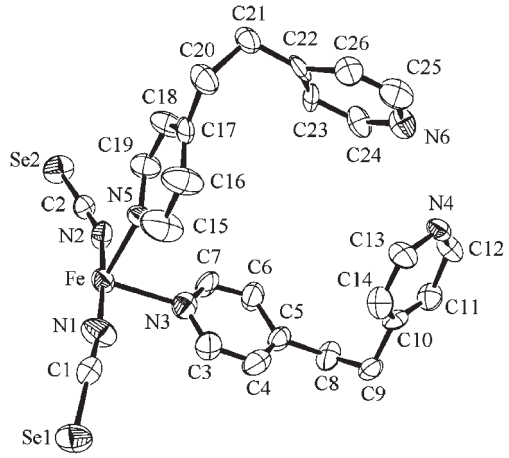

Fig. 3. ORTEP drawing of the 1D structure of $[Fe(NCSe)_2(bpa)_2]$ at 130 K.

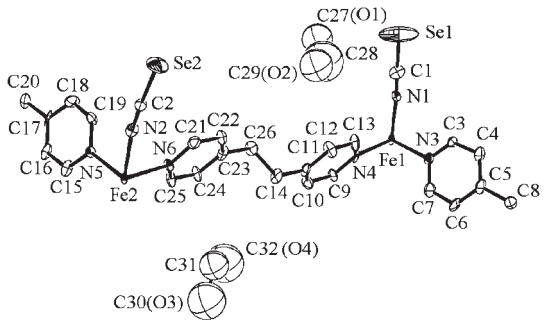

Fig. 4. ORTEP drawing of the interpenetration structure of $[Fe(NCSe)_2(bpa)_2]\cdot EtOH$ at 130 K. The position of the oxygen atom is not determined, because the EtOH molecule is disordered in the two positions.

In the case of NCSe, 1D and interpenetration structures were obtained. Figures 3 and 4 show the ORTEP drawings of the 1D and interpenetration structures of the NCSe complexes, respectively. The crystallographic data are shown in Table 1. The selected bond distances and angles are shown in Tables 4 and 5, respectively. The 1D structure consists of a *gauche* isomer of bpa, while the interpenetration structure consists of an *anti* isomer of bpa. The solvent molecule is not included in the 1D structure, while it is included in the interpenetration structure. The solvent molecules are disordered. These contrasts are similar to the case of the corresponding NCS complexes. The iron atoms are coordinated by four pyridine nitrogen donors and two selenocyanate nitrogen donors. The *cis* N–Fe–N bond angles deviate slightly from 90° in both crystals, indicative of a slightly distorted environment in both crystals. The NCSe ligands coordinate to the Fe atom in a bent fashion with the angles of 157(1) and 155(1)° in the 1D structure, while in almost a parallel fashion with the angles of 175(1) and 171(1)° in the interpenetration structure. The NCSe ligands themselves are almost linear both in the 1D and inter-

penetration structures. The Fe–N(NCSe) and Fe–N(bpa) distances are also typical values in the Fe^{II} high-spin complexes.

Figure 5 shows typical ^{57}Fe Mössbauer spectra at 78 K. From the spectra, the isomer shift (IS) and quadrupole splitting (QS) values were calculated. All the ^{57}Fe Mössbauer parameters are summarized in Table 6. All the spectra showed about 1.1 mm s^{-1} for the IS value. The IS value around 1.1 mm s^{-1} reveals a high-spin Fe^{II} state. This reveals that there is good agreement with the Fe–N distances obtained from X-ray structural analyses. The Mössbauer parameter is slightly affected by changing the included solvent in the same interpenetration structure. The spectrum of Fig. 5b shows a small amount of a larger QS doublet, which is attributed to contamination from the 1D structure crystals. It can easily be seen that the QS value changes drastically depending on the structure and

Table 4. Selected Bond Distances (Å) and Angles (°) for the 1D Structure of $[Fe(NCSe)_2(bpa)_2]$

Fe1–N1	2.14(2)	Fe1–N2	2.16(2)
Fe1–N3	2.27(1)	Fe1–N4[a)]	2.27(1)
Fe1–N5	2.20(1)	Fe1–N6[a)]	2.21(1)
N1–Fe1–N3	93.9(6)	N1–Fe1–N4[a)]	86.2(7)
N1–Fe1–N5	90.0(6)	N1–Fe1–N6[a)]	92.3(7)
N2–Fe1–N3	88.6(6)	N2–Fe1–N4[a)]	90.2(7)
N2–Fe1–N5	93.7(6)	N2–Fe1–N6[a)]	85.2(7)
N3–Fe1–N4[a)]	90.5(5)	N3–Fe1–N5	87.3(4)
N4[a)]–Fe1–N6[a)]	90.1(5)	N5–Fe1–N6[a)]	92.5(5)
N1[a)]–Fe1–N2[b)]	175.6(5)	N3–Fe1–N6[a)]	173.7(8)
N4[a)]–Fe1–N5	175.5(6)	Fe1–N1–C1	157(1)
Fe1–N2–C2	155(1)	N1–C1–Se1	178(1)
N2–C2–Se2	178(1)		

a) Symmetry operator: x, $y+1$, z. b) Symmetry operator: x, $y-1$, z.

Table 5. Selected Bond Distances (Å) and Angles (°) for the Interpenetration Structure of $[Fe(NCSe)_2(bpa)_2]\cdot EtOH$

Fe1–N1	2.13(1)	Fe1–N3	2.23(1)
Fe1–N4	2.24(1)	Fe2–N2	2.15(1)
Fe2–N5	2.23(1)	Fe2–N6	2.24(1)
N1–Fe1–N3	88.6(4)	N1–Fe1–N4	91.3(4)
N3–Fe1–N4	87.7(4)	N2–Fe2–N5	90.4(4)
N2–Fe2–N6	89.2(4)	N5–Fe2–N6	87.6(4)
Fe1–N1–C1	175(1)	Fe2–N2–C2	171(1)
N1–C1–Se1	179(1)	N2–C2–Se2	176(1)

Table 6. ^{57}Fe Mössbauer Parameters for Several Structures of $[Fe(NCX)_2(bpa)_2]$ (X = S and Se)

Sample	T/K	IS[a)]/mm s^{-1}	QS/mm s^{-1}
$[Fe(NCS)_2(bpa)_2]$	298	1.06	1.60
(1D structure)	78	1.18	2.17
$[Fe(NCS)_2(bpa)_2]\cdot EtOH$	78	1.18	0.96
(2D grid structure)			
$[Fe(NCS)_2(bpa)_2]\cdot EtOH$	78	1.16	1.02
(Interpenetration structure)			
$[Fe(NCS)_2(bpa)_2]\cdot PrOH$	298	1.07	0.87
(Interpenetration structure)	78	1.17	1.14
$[Fe(NCSe)_2(bpa)_2]$	298	1.04	0.69
(1D structure)	78	1.18	0.74
$[Fe(NCSe)_2(bpa)_2]\cdot EtOH$	78	1.19	1.53
(Interpenetration structure)			
Time dependence of $[Fe(NCS)_2(bpa)_2]\cdot PrOH$			
(Interpenetration structure)			
(fresh)	298	1.07	0.87
(18 days later)	298	1.06	0.94
		1.05	1.69
(26 days later)	298	1.06	1.69
		1.05	2.15

a) Relative to iron foil.

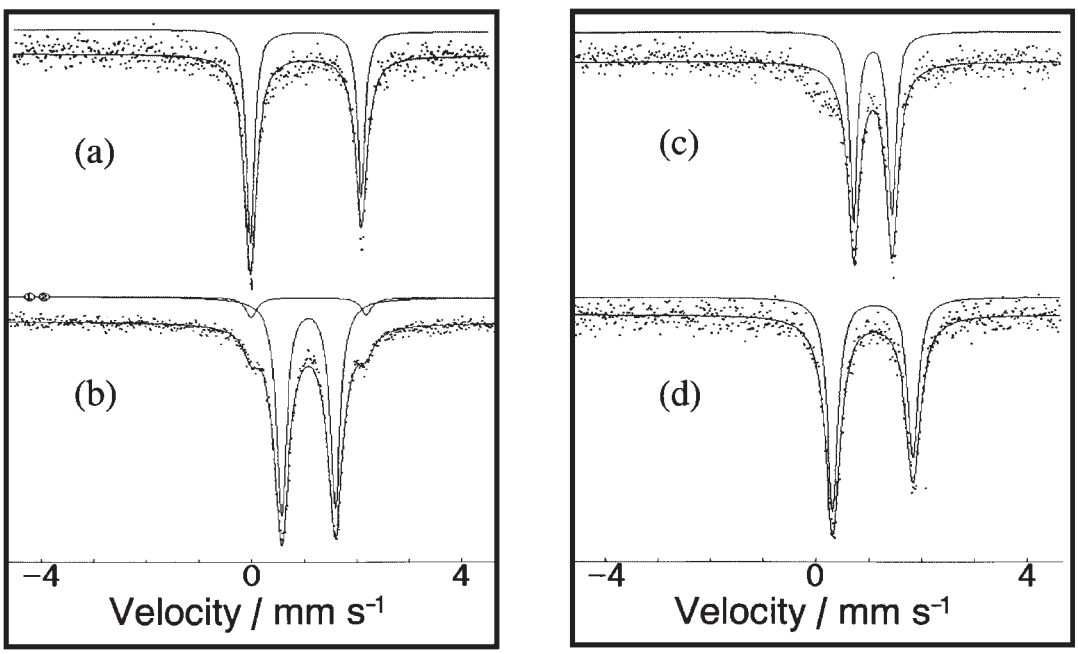

Fig. 5. Typical ^{57}Fe Mössbauer spectra at 78 K of the (a) 1D structure of $[Fe(NCS)_2(bpa)_2]$, (b) interpenetration structure of $[Fe(NCS)_2(bpa)_2]\cdot EtOH$, (c) 1D structure of $[Fe(NCSe)_2(bpa)_2]$, and (d) interpenetration structure of $[Fe(NCSe)_2(bpa)_2]\cdot EtOH$.

anion. In the NCS complex, the QS value (2.17 mm s^{-1}) for the 1D structure is two times larger than that (1.02 or 1.14 mm s^{-1}) for the interpenetration structure. On the other hand, in the NCSe complex, the QS value (0.74 mm s^{-1}) for the 1D structure is half of that (1.53 mm s^{-1}) for the interpenetration structure. The structure dependence of the QS value appeared conversely between NCS and NCSe complexes. Definitely, this can not be explained by only the anion effect. The smaller QS values were compared between NCS and NCSe complexes and also the larger QS values were compared between them. From these comparisons, the NCSe complexes showed smaller QS values compared with the corresponding NCS complexes. This trend is also observed in similar assembled complexes[32] and mononuclear complexes[33] of FeN_6 arrangement.

In $[FeCl_2(py)_2]$, it is known that the QS value changes result from a slight change of structure.[34] We compared the environment around the iron atom among all structures. X-ray structural analyses revealed that the two NCS or NCSe ligands coordinate to the iron atom in a *trans* fashion. There are no significant differences in the bond length of Fe–N in all isomers and between NCS and NCSe complexes. There are also no significant differences in the coordination angles of the ligand between NCS and NCSe complexes, although the difference in coordination angles of the bpa ligand is seen between the 1D and interpenetration structure. Therefore, the change in the Mössbauer spectra can not be explained by only the structural change around the iron atom. Nevertheless, a drastic change in the QS value is observed by changing the structure and by changing NCS to NCSe. To explain the present results, we have to consider both the structure effect and anion effect. One of the possibilities to explain all the changes in the QS value is to introduce a reverse sign of the electric field gradient (EFG) by changing NCS to NCSe in the same structure and by changing the structure in the same anion, because the contribution of the d_{xy} electron to EFG is two times larger than that of the d_{yz} or d_{xz} electron.[35] A detailed explanation is under study.

A large difference in the QS value of the ^{57}Fe Mössbauer spectra between the structures may play a powerful role in investigating solid-to-solid phase transformation. Figure 6 shows the time dependence of the ^{57}Fe Mössbauer spectra of $[Fe(NCS)_2(bpa)_2]\cdot$PrOH having interpenetration structure at 298 K. The sample is wrapped up with the hydrocarbon at room temperature; otherwise, the crystals would be destroyed quickly. Actually, the destruction is easily seen without the hydrocarbon. The small QS value of the fresh sample of the interpenetration structure is a typical feature of this structure. The larger QS doublet (1.69 mm s^{-1}) appeared in addition to the smaller one in a sample that stood at room temperature for 18 days. In a sample that stood at room temperature for 26 days, the initial smaller QS doublet disappeared and the larger QS doublet (1.69 mm s^{-1}) became a main component with the largest QS species (2.15 mm s^{-1}). The species having the largest QS value is not understood. Although the larger QS value (1.69 mm s^{-1}) is close to the value of the 1D structure of the NCS complex, the powder X-ray diffraction pattern of the sample after the Mössbauer measurement revealed it to be relatively similar to the original structure.

Figure 7a shows the temperature dependence of the powder X-ray diffraction patterns of $[Fe(NCS)_2(bpa)_2]\cdot$EtOH under a nitrogen atmosphere. The powder X-ray diffraction pattern of the initial sample from single crystals of interpenetration structure shows a change with increasing temperature. The pattern at room temperature is of typical interpenetration type. At 325 K, a new pattern superimposed on the original one. The pattern at 350 K is apparently different from the original one, which is the same as the simulation pattern of 1D structure. Figure 7b shows the temperature dependence of the powder X-ray diffraction patterns of $[Fe(NCS)_2(bpa)_2]\cdot$PrOH under a nitrogen atmosphere. The sample is a powder of single crystals of interpenetration structure. A similar temperature dependence with $[Fe(NCS)_2(bpa)_2]\cdot$EtOH is observed. The transition temperature is higher than $[Fe(NCS)_2(bpa)_2]\cdot$EtOH maybe because of the larger mass of PrOH. The results reveal a transformation from interpenetration structure to the 1D one. Close inspection of the pattern around the transition temperature both in $[Fe(NCS)_2(bpa)_2]\cdot$EtOH and $[Fe(NCS)_2(bpa)_2]\cdot$PrOH reveals that the new pattern exists in addition to the original and final patterns. This reveals that the transition from interpenetration structure to 1D structure is not a one-step process but a two-step process. New diffraction observed around the transition temperature is thought to be due to an intermediate structure. We can imagine that the desolvation and structural change do not occur simultaneously. It is supposed that the structural change from the interpenetration structure to 1D structure occurs after the desolvation. From this consider-

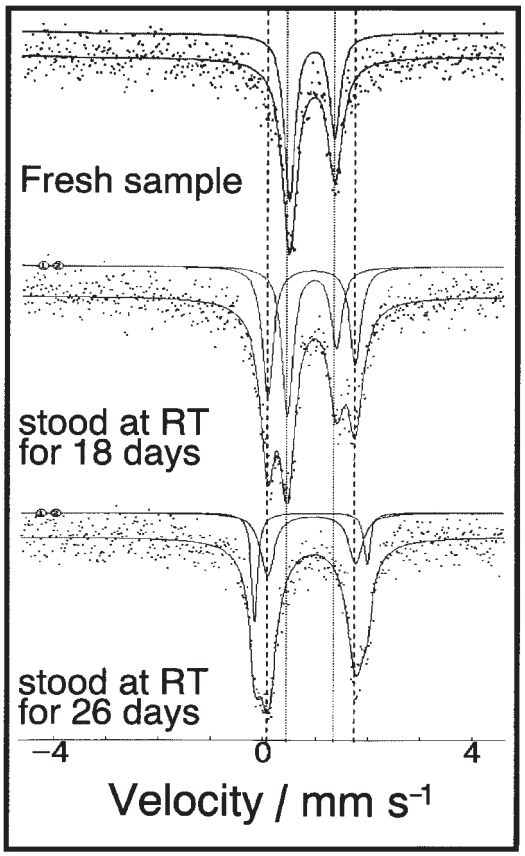

Fig. 6. Time dependence of the ^{57}Fe Mössbauer spectra at 298 K for the sample obtained as the interpenetration structure of $[Fe(NCS)_2(bpa)_2]\cdot$PrOH.

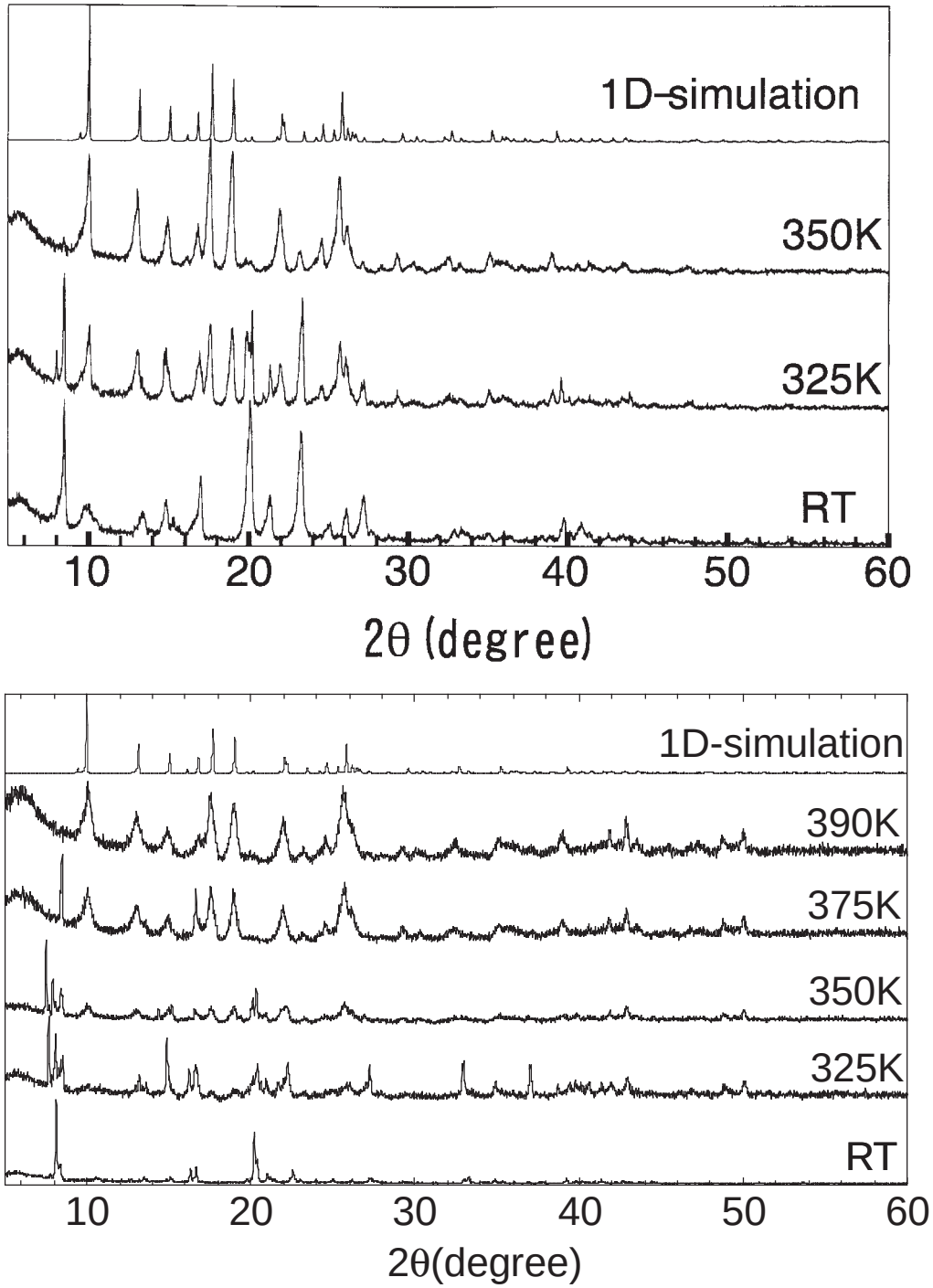

Fig. 7. Temperature dependence of the powder X-ray diffraction patterns of the interpenetration structure of (a) $[Fe(NCS)_2(bpa)_2]\cdot EtOH$ (upper) and (b) $[Fe(NCS)_2(bpa)_2]\cdot PrOH$ (bottom).

ation, it is thought that the larger QS doublet ($1.69\,mm\,s^{-1}$) in Fig. 6 is due to the strained structure after desolvation. The strain of framework by desolvation may cause the change in QS. We confirmed that the single crystals of interpenetration structure changed to the 1D structure by keeping the sample for longer time at room temperature. Collapsing of the crystal structure by releasing the solvent molecule is well known.[15] Many inclusion coordination compounds irreversibly lose crystallinity. In the present case, the phase transformation of the interpenetration structure to the 1D structure is observed after removing the solvent molecule.

We obtained the powder sample by mixing the starting materials quickly. The structure is known to be the 1D structure. However, there is a possibility to have an interpenetration structure. The present result, however, reveals that the interpenetration structure will change quickly to the 1D structure, even though the interpenetration structure is obtained in the preparation of the powder sample.

Conclusion

Three supramolecular isomers of an Fe–NCS complex and two isomers of an Fe–NCSe complex bridged by bpa were obtained. 2D grid and interpenetration structures for the NCS complexes and 1D and interpenetration structures for the NCSe complexes were new structures. ^{57}Fe Mössbauer spectroscopy revealed that the present sample is in a high-spin state and drastic change in the QS value occurs by changing the structure and by changing NCS to NCSe. The solid-to-solid transformation phenomenon was observed, accompanied by a drastic change in the QS value. The structural change was easily observed by heating the sample. The present phase transformation accompanied by a drastic change in the QS value is unprecedented and attractive for achieving new functionality.

References

1 B. F. Hoskins, R. Robson, *J. Am. Chem. Soc.* **1990**, *112*, 1546.

2 R. G. Gable, B. F. Hoskins, R. Robson, *J. Chem. Soc., Chem. Commun.* **1990**, 1677.

3 T. Kitazawa, S. Nishikiori, R. Kuroda, T. Iwamoto, *J. Chem. Soc., Dalton Trans.* **1994**, 1029.

4 M. Fujita, Y. J. Kwon, S. Washizu, K. Ogura, *J. Am. Chem. Soc.* **1994**, *116*, 1151.

5 S. Kawata, S. Kitagawa, M. Kondo, I. Furuchi, M. Munakata, *Angew. Chem., Int. Ed. Engl.* **1994**, *33*, 1759.

6 X.-M. Chen, M.-L. Tong, Y.-J. Luo, Z.-N. Chen, *Aust. J. Chem.* **1996**, *49*, 835.

7 A. J. Blake, S. J. Hill, P. Hubberstey, W.-S. Li, *J. Chem. Soc., Dalton Trans.* **1997**, 913.

8 L. Carlucci, G. Ciani, D. M. Proserpio, A. Sironi, *J. Chem. Soc., Dalton Trans.* **1997**, 1801.

9 M.-L. Tong, X.-M. Chen, X.-L. Yu, T. C. W. Mak, *J. Chem. Soc., Dalton Trans.* **1998**, 5.

10 L. R. MacGillivray, R. H. Groeneman, J. L. Atwood, *J. Am. Chem. Soc.* **1998**, *120*, 2676.

11 B. Moulton, M. J. Zaworotko, *Chem. Rev.* **2001**, *101*, 1629.

12 T. L. Hennigar, D. C. MacQuarrie, P. Losier, R. D. Rogers, M. J. Zaworotko, *Angew. Chem., Int. Ed. Engl.* **1997**, *36*, 972.

13 S. Noro, R. Kitaura, M. Kondo, S. Kitagawa, T. Ishii, H. Matsuzaka, M. Yamashita, *J. Am. Chem. Soc.* **2002**, *124*, 2568.

14 S. Noro, M. Kondo, T. Ishii, S. Kitagawa, H. Matsuzaka, *J. Chem. Soc., Dalton Trans.* **1999**, 1569.

15 S. Kitagawa, M. Kondo, *Bull. Chem. Soc. Jpn.* **1998**, *71*, 1739.

16 M. Schweiger, S. R. Seidel, A. M. Arif, P. J. Stang, *Inorg. Chem.* **2002**, *41*, 2556.

17 M. L. Hernández, M. G. Barandika, M. K. Urtiaga, R. Cortés, L. Lezama, M. I. Arriortua, T. Rojo, *J. Chem. Soc., Dalton Trans.* **1999**, 1401.

18 M. L. Hernández, M. K. Urtiaga, M. G. Barandika, R. Cortés, L. Lezama, N. de la Pinta, M. I. Arriortua, T. Rojo, *J. Chem. Soc., Dalton Trans.* **2001**, 3010.

19 J. Lu, T. Paliwala, S. C. Lim, C. Yu, T. Niu, A. J. Jacobson, *Inorg. Chem.* **1997**, *36*, 923.

20 D. Czakis-Sulikowska, J. Kałużna-Czaplińska, *J. Therm. Anal. Calorim.* **2000**, *62*, 821.

21 M. Kondo, Y. Shimizu, M. Miyazawa, Y. Irie, A. Nakamura, T. Naito, K. Maeda, F. Uchida, T. Nakamoto, A. Inaba, *Chem. Lett.* **2004**, *33*, 514.

22 T. Kitazawa, U. Gomi, M. Takahashi, M. Takeda, M. Enomoto, A. Miyazaki, T. Enoki, *J. Mater. Chem.* **1996**, *6*, 119.

23 E. Breuning, M. Ruben, J. M. Lehn, F. Renz, Y. Garcia, V. Ksenofontov, P. Gütlich, E. Wegelius, K. Rissanen, *Angew. Chem., Int. Ed.* **2000**, *39*, 2504.

24 J. A. Real, E. Andrés, M. C. Muñoz, M. Julve, T. Granier, A. Bousseksou, F. Varret, *Science* **1995**, *268*, 265.

25 N. Moliner, M. C. Muñoz, S. Létard, L. Salmon, J.-P. Tuchagues, A. Bousseksou, J. A. Real, *Inorg. Chem.* **2002**, *41*, 6997.

26 G. J. Halder, C. J. Kepert, B. Moubaraki, K. S. Murray, J. D. Cashion, *Science* **2002**, *298*, 1762.

27 S. Nakashima, A. Yamamoto, Y. Asada, N. Koga, T. Okuda, *Inorg. Chim. Acta* **2005**, *358*, 257.

28 M. Febbinteanu, G. Marinescu, H. W. Roesky, M. Noltemeyer, H.-G. Schmidt, M. Andruh, *Polyhedron* **1999**, *18*, 243.

29 MacDENZO: D. Gewrth (with the cooperation of the program authors Z. Otwinowski, M. Minor), in *The MacDenzo Manual—A Description of the Programs DENZO, XDISPLAYF, and SCALEPACK*, Yale University, New Haven, CT, **1995**.

30 CrystalStructure 2.00: *Crystal Structure Analysis Package*, Rigaku and MSC, **2001**.

31 CRYSTALS Issue 10: D. J. Watkin, C. K. Prout, J. R. Carruthers, P. W. Betterudge, Chemical Crystallography Laboratory, Oxford, UK.

32 S. Nakashima, Y. Asada, T. Okuda, *Hyperfine Interact.* **2004**, *156/157*, 353.

33 B. F. Little, G. J. Long, *Inorg. Chem.* **1978**, *17*, 3401.

34 a) H. Sano, M. Kanno, *Chem. Lett.* **1973**, 127. b) G. J. Long, D. L. Whitney, J. K. Kennedy, *Inorg. Chem.* **1971**, *10*, 1406. c) P. J. Clark, H. J. Milledge, *Acta Crystallogr., Sect. B* **1975**, *31*, 1543.

35 T. C. Gibb, *Principles of Mössbauer Spectroscopy*, Chapman and Hall, London, **1977**.